A sharp degree bound on G^2-refinable multi-sided surfaces

Kęstutis Karčiauskas[a], Jörg Peters[b,*]

Department CISE, University of Florida

[a] *Vilnius University, Lithuania*
[b] *University of Florida, USA*

Abstract

Refinement of a space of splines should yield additional degrees of freedom for modeling and engineering analysis, both along boundaries and in the interior. Yet such additional flexibility fails to materialize for multi-sided G^2 surface constructions when the polynomial degree is too low.

This paper establishes a tight lower bound on the polynomial degree of flexibility-increasing refinable multi-sided G^2 surface constructions within a C^2 spline complex – by ruling out bi-5 constructions and by exhibiting a multi-sided bi-6 construction that yields good highlight line and curvature distributions. The bi-6 construction consists of one 2×2 macro-patch for each of the n sectors that join to form the multi-sided surface

Keywords: flexibility-increasing, refinement, generalized spline, multi-sided, lower bound, free-form surface, good shape

1. Introduction

Where more than two parameter lines cross and therefore $n \neq 4$ surface patches (sectors) meet at an extraordinary point, the surface parameters have to adapt to avoid a singularity. Any such change of variables connects derivatives along and across the n sector-separating curves that emanate from the extraordinary point. When the polynomial degree is too low compared to the smoothness between the sectors, patches fuse in the sense that, what should be a piecewise polynomial with many degrees of freedom, becomes a single polynomial.

This failure to produce new linearly independent local basis functions not only prevents the geometry from becoming more flexible, but also impairs the convergence of functions on the surface. For example, when solving differential equations, [1] showed that C^2-connected bi-cubics have a sub-optimal approximation order in the presence of extraordinary points and, more generally, that h-refinement in the presence of non-trivial reparameterizations fuses piecewise polynomials of degree p when the continuity is C^{p-1}. Earlier [2] showed that for bi-3 (bicubic) spline patches the interdependence of partial derivatives forces a minimum separation of the extraordinary points when polynomial pieces are joined G^1. Both [1] and [3] recommend constructions of degree bi-4 to avoid artificial stiffness or 'locking' under G^1-refinability.

This paper focuses on refinement of multi-sided G^2 surface caps consisting of a finite number of pieces and without singular parameterization. Concretely, this paper

- proves that there is no flexibility-increasing refinable bi-5 construction completing a C^2 spline complex by a G^2 cap with C^2 sectors;
- exhibits a bi-6 construction with 2×2 pieces per sector such that the surfaces have good highlight line and curvature distributions; and
- shows that the bi-6 construction is refinable with increasing flexibility along all boundaries and in the interior of all sectors.

The flexibility-increasing construction can represent both the physical domain and finer functions on this domain for engineering analysis.

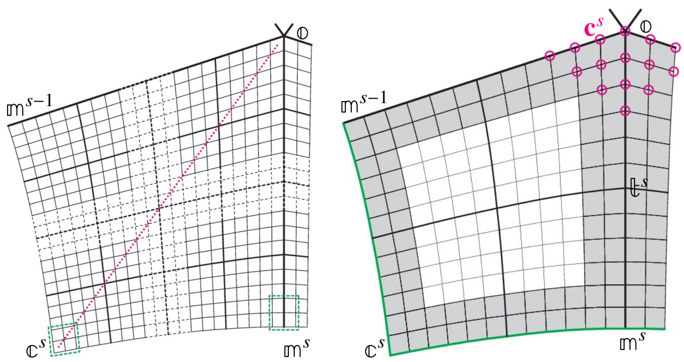

(a) macro-patch bi-5 G^2 (b) refinable 2×2 bi-6 G^2

Figure 1: Layout of pieces and their BB-nets of (a) a hypothetical bi-5 construction with internally C^2 macro-patches. Such constructions fail to be flexibility-increasing G^2-refinable, regardless of the number of pieces; (b) the 2×2 bi-6 macro-patch constructions of Section 4. The BB-coefficients marked ∘ represent the cubic expansion, $\mathbf{c}^s$ in sector s. The extraordinary point is marked $\mathbb{o}$, corner points $\mathbb{c}^s$ and midpoints $\mathbb{m}^s$ of a sector s.

1.1. Related literature

On regular, non-multi-sided or multi-patch mesh configurations, the practice of using the same bi-variate tensor-product (hence refinable) splines, both for modeling the geometry of the domain and for computing functions on this domain, goes back at least to [4] and has been regularly advocated and advanced in the literature [5, 6, 7, 8]. This consistent use of splines is also the central tenet of iso-geometric analysis [9]. For C^1 elements,

*Corresponding author
Email addresses: kestutis.karciauskas@mif.vu.lt (Kęstutis Karčiauskas), jorg.peters@gmail.com (Jörg Peters)

the inclusion of irregular configurations into matching geometry and analysis spline spaces was pioneered in [10, 11, 12, 13] and applied to planar multi-patch domains in [14]. [15] considers C^2 elements on the union of two bi-linear domains. The present paper derives a G^2 construction not restricted to bilinear but suitable for inclusion into any bi-cubic C^2 spline complex. The resulting surfaces are typically of good shape. By the result in [16] such a space provides C^2 elements for engineering analysis.

The G^2 constructions in [17] (of degree bi-7) and [18] (of degree bi-6) can also generate good shape but are not G^2 refinable. Constructions like [19] do not gain flexibility since their shape is fixed by composition with a fixed (quadratic or cubic) map. The C^2-refinable construction of [20] is of degree bi-9 and has shape restrictions that make it unsuitable for high-end design.

Overview. Section 2 defines the surface representation and the notions of smoothness and flexibility-increasing refinement. Section 3 establishes the lower bound by showing that multi-sided bi-5 G^2 constructions can not be flexibility-increasing. Section 4 presents a bi-6 G^2 construction for multi-sided caps, suitable for inclusion into a C^2 spline complex, that Section 5 shows to be G^2 and flexibility-increasing refinable. Alternatives and design choices are discussed in Section 6.

2. Definitions and Setup

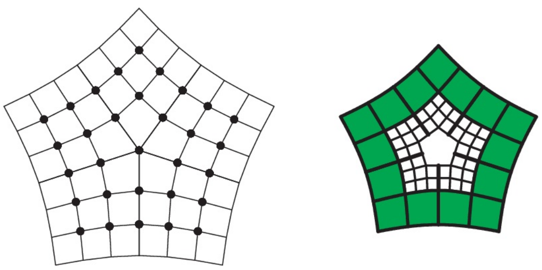

(a) B-spline-like control points (b) ring and tensor-border

Figure 2: (from [13]) (a) Input net of B-spline-like control points • of independent G^2 functions. (b) The full input net defines a ring of C^2-connected bicubic patches. The subnet of points marked • in (a) define a C^2-extension shown as the finer inner mesh on white background (representing the BB-net of coefficients in Bernstein-Bézier form). The subnet defines the multi-sided surface cap.

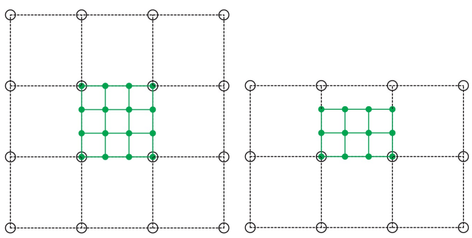

(a) bi-3 patch $\mathbf{p}$ (b) tensor-border

Figure 3: Bi-3 B-to-BB conversion. Circles ◦ mark B-spline control points, solid disks • mark BB-coefficients.

The multi-sided surfaces will be a collection of tensor-product patches of bi-degree d (short bi-d) in Bernstein-Bézier form (BB-form), see e.g. [21]:

$$\mathbf{f}(u,v) := \sum_{k=0}^{d}\sum_{\ell=0}^{d} \mathbf{f}_{k\ell} B_k^d(u) B_\ell^d(v), \quad (u,v) \in [0..1]^2.$$

Here $B_i^d(t) := \binom{d}{i}(1-t)^{d-i}t^i$ are the Bernstein polynomials of degree d and $\mathbf{f}_{ij}$ are the BB-coefficients. We abbreviate $\mathbf{f} := \sum_{k=0}^{d} \mathbf{f}_k B_k^d$ as

$$\mathbf{f} \sim [\mathbf{f}_0, \ldots, \mathbf{f}_d]$$

and define the *layer curves* $\mathbf{f}_j \sim [\mathbf{f}_{0j}, \ldots, \mathbf{f}_{dj}]$. Connecting $\mathbf{f}_{ij}$ to $\mathbf{f}_{i+1,j}$ and $\mathbf{f}_{i,j+1}$ wherever possible yields the *BB-net*. A useful operation on polynomials in BB-form is to split them into two pieces, say a left half and a right half, by the well-known *de Casteljau algorithm* [21].

The vertices of any 4×4 sub-grid in the mesh, such as the grey net in Fig. 3 a, can be interpreted as the control net of a uniform bi-3 B-spline [22]. The *B-to-BB conversion* expresses the spline in bi-3 BB-form illustrated by the green BB-net in Fig. 3 a. A partial conversion from a partial mesh yields a sub-net of the BB-net. A sub-net defining position, first and second derivatives across an edge Fig. 3 b is called a *tensor-border*.

Definition 1 (G^2 constraints). *Two surface pieces $\tilde{\mathbf{f}}, \mathbf{f} : (u,v) \in \mathbb{R}^2 \to \mathbb{R}^d$ that share a boundary curve* $\mathbf{e}$ join G^2 along $\mathbf{e}$ *if there exists a suitably oriented and non-singular reparameterization $\rho : \mathbb{R}^2 \to \mathbb{R}^2$ so that the partial derivatives $\partial^k\tilde{\mathbf{f}}$ and $\partial^k(\mathbf{f}\circ\rho)$, $k = 0,1,2$, agree along* $\mathbf{e}$.

Throughout, we will choose $\mathbf{e}$ to correspond to surface patch parameters $(u, 0 = v)$. Then the relevant Taylor expansion (up to degree 2) of the reparameterization ρ with respect to v is

$$\rho(u,v) := (u + b(u)v + \frac{1}{2}e(u)v^2,\ a(u)v + \frac{1}{2}d(u)v^2). \tag{1}$$

The chain rule of differentiation yields the well-known G^1 and G^2 constraints on constructions in terms of univariate scalar maps $a, b, d, e : u \in \mathbb{R} \to \mathbb{R}$ and the vector-valued functions $\mathbf{f}(u,0)$, $\tilde{\mathbf{f}}(u,0)$:

$$\partial_v\tilde{\mathbf{f}} = a\,\partial_v\mathbf{f} + b\,\partial_u\mathbf{f}, \tag{2}$$
$$\partial^2_{vv}\tilde{\mathbf{f}} = a^2\,\partial^2_{vv}\mathbf{f} + 2a\,b\,\partial_u\partial_v\mathbf{f} + b^2\,\partial^2_{uu}\mathbf{f} + d\,\partial_v\mathbf{f} + e\,\partial_u\mathbf{f}. \tag{3}$$

If $a(u) := 1$, $b(u) := 0$, $d(u) := 0$ and $e(u) := 0$ then $\rho(u,v)$ reduces to identity map and the G^2 constraints are called (parametric) C^2 constraints.

Considering n surface sectors surrounding a central point, the sectors are constructed *diagonally symmetric* if the formulas that define $\mathbf{f}_{ji}$ can be obtained from those defining $\mathbf{f}_{ij}$ by exchanging i and j. The construction is *unbiased* if, when $\tilde{\mathbf{f}}$ and $\mathbf{f}$ are exchanged in (2) or (3), the constraints remain the same. No bias implies

$$a(u) := -1 \text{ and } e(u) := b(u)(b'(u) - \frac{d(u)}{2}). \tag{4}$$

Since, for any reasonable construction, input symmetry should be preserved and the output should be invariant under re-labeling, diagonal construction symmetry and no bias are reasonable requirements for any general construction.

G-spline spaces and refinement. If we specify a reparameterization $\rho_{\mathbf{e}}$ for every edge $\mathbf{e}$ then a space G_ρ of tensor-product BB-patches joined with the same reparameterizations forms a linear vector space in the unconstrained BB-coefficients. That is, any linear combination of elements in G_ρ is again in G_ρ.

The space G_ρ is *refinable* to a space $\dot{G}_{\dot{\rho}}$ in the following sense, see Fig. 4 . For each polynomial piece $\mathbf{f} \in G_\rho$ defined on $\square := [0..1]^2$, the space $\dot{G}_{\dot{\rho}}$ has four polynomial pieces $\mathbf{f}^r$, $r = 1,2,3,4$

(wlog. of the same degree as $\mathbf{f}$) defined on the four quarters of $\square$ and joined by the following reparameterizations $\dot\rho$: the Taylor expansion $\dot\rho$ up to degree 2 across the new four inner edges $\dot\rho$ is the identity, i.e. the pieces join C^2; along any original edge $\mathbf{e}^p$ ρ is retained in pieces:

$$\dot\rho_{\mathbf{e}^{p,0}}(u,v) = \rho_{\mathbf{e}^p}(\frac{u}{2},\frac{v}{2}), \quad \dot\rho_{\mathbf{e}^{p,1}}(u,v) = \rho_{\mathbf{e}^p}(\frac{1}{2}+\frac{u}{2},\frac{v}{2}).$$

Then there is a choice of $\mathbf{f}^r$, namely applying de Casteljau's algorithm to $\mathbf{f}$ at $u = v = 1/2$, so that any element $\mathbf{f} \in G_\rho$ can be represented in $\dot G_{\dot\rho}$. That is, $\dot G_{\dot\rho}$ refines G_ρ. However, many other choices of macro-patches $\mathbf{f}^r$ are allowable so that $\dot G_{\dot\rho}$ can be expected to provide more flexibility than G_ρ, i.e. has more degrees of freedom, e.g. BB-coefficients not constrained by enforcing smoothness.

Definition 2 (flexibility-increasing refinable). *With the preceding definition of $\dot G_{\dot\rho} \supsetneq G_\rho$ a construction is* flexibility-increasing refinable *if, for each domain piece $\square$, $\dot G_{\dot\rho}$ has more degrees of freedom than G_ρ, both along map boundaries and in the interior.*

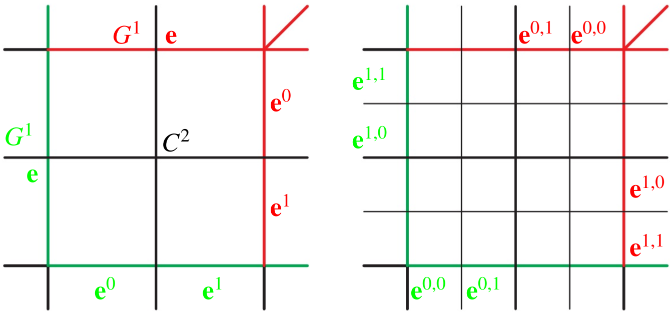

(a) initial (b) refined

Figure 4: G-spline refinement. To be flexibility-increasing, new degrees of freedom must appear both in the interior and along the red sector-separating curve boundaries and the green boundaries that connect the cap to the remaining surface.

In this paper, we focus on multi-sided caps whose sectors are internally C^2. That is the black transitions in Fig. 4 are C^2. In the context of refinement it is natural to focus on internally C^2 sectors since all new internal transitions arising from refinement must be parametrically C^2 to reproduce the original polynomial pieces by the finer construction. Moreover, constructions with internally G^2 sectors are not only more complicated, but, in our experience, yield lower surface quality.

In the next section, we will see that refined functions can remain a single polynomial along the reparameterized G-edges, i.e. the expected additional dofs fail to materialize under refinement. In [1] such lack of new flexibility was called 'locking' in analogy to a term in engineering shell computation.

3. Unbiased, diagonally-symmetric multi-sided G^2 bi-5 constructions are not flexibility-increasing refinable

This section establishes that diagonally symmetric and unbiased G^2 constructions of multi-sided surfaces with C^2 sectors must have degree higher than bi-5 in order for their refinement to be flexibility-increasing. The proof consists of multiple steps,

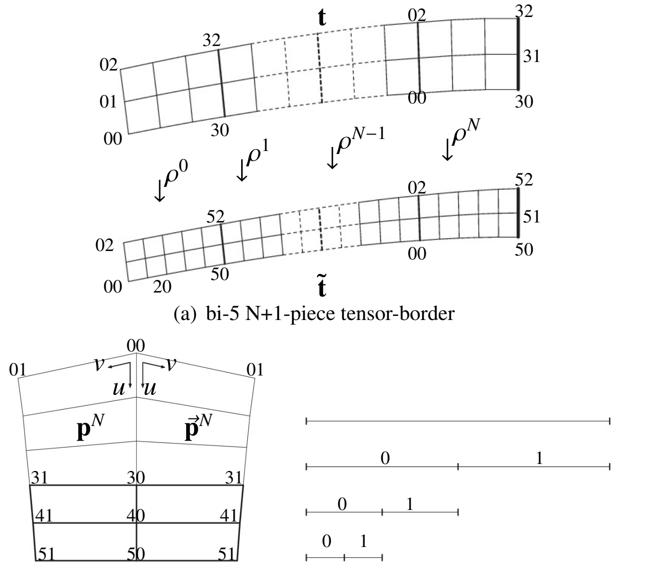

(a) bi-5 N+1-piece tensor-border

(b) adjacent sectors (c) binary refinement (leftmost part)

Figure 5: Bi-5 construction. (a) Reparameterization of any N+1-piece C^2 input tensor-border $\mathbf{t}$. (b) G^1-join of neighbor sectors sharing the tensor border. (c) from top. Row 1: initial piece $\mathbf{t}^k$, row 2: first split, row 3, 4: left parts of subsequent splits.

condensed in lemmas and corollaries, that are each conceptually simple, but were originally discovered by symbolic computation.

Connecting the sectors of a finite multi-sided construction G^2 requires a careful choice of *reparameterization along the input boundary* $\mathbb{c}, \mathbb{m}$ in order to also meet the surrounding surface with second-order smoothness. Fig. 5 a depicts a uniform split of the tensor-border $\mathbf{t}$ of one sector (cf. Fig. 2 b) into $N+1$ pieces $\mathbf{t}^k$, $k = 0, 1, \ldots, N$. Each piece is reparametrized by ρ^k defined in terms of local functions a^k, b^k, d^k, e^k in (1) to yield new tensor-borders $\tilde{\mathbf{t}}^k$.

Proposition 1. *For an unbiased G^2 construction,*

(i) across $\mathbb{c}^s, \mathbb{m}^s$, the functions a, b, d, e of ρ must be polynomials;

(ii) across $\mathbb{m}^s, \mathbb{o}$, $a \equiv -1$ and b must be a polynomial.

We recall that unbiased constructions require $a(u) \equiv -1$. The remaining proof of Prop. 1 is in Appendix C.

Lemma 1 (degree bounds of ρ across $\mathbb{c}, \mathbb{m}$). *If the tensor-borders $\mathbf{t}$ are of degree bi-3 and the reparameterized tensor-borders $\tilde{\mathbf{t}}^k$ are of degree bi-5 then the polynomial degree of a^k, b^k, d^k, e^k is respectively less or equal to 1, 2, 2, 3.*

Proof Let $\mathtt{deg}(h)$ denote a degree of function h in u-direction. Counting confirms that the stated choice of degrees yields tensor-borders $\tilde{\mathbf{t}}^s$ of degree 5 in the u-direction. To show that the listed degrees are maximal, replace in (2) and (3) $\mathbf{f}$ by $\mathbf{t}^k$ and $\tilde{\mathbf{f}}$ by $\tilde{\mathbf{t}}^k$. Then (2) implies that $5 = \mathtt{deg}(\partial_v \tilde{\mathbf{t}}^k) = \max\{\mathtt{deg}(a^k\partial_v\mathbf{t}^k), \mathtt{deg}(b^k\partial_u\mathbf{t}^k)\} = \max\{\mathtt{deg}(a^k)+3, \mathtt{deg}(b^k)+2\}$ and therefore $\mathtt{deg}(a^k) \leq 2$ and $\mathtt{deg}(b^k) \leq 3$. We next use the fact that the $3\times(3+1)$ BB-coefficients of $\mathbf{t}$ are *linearly independent* and we can choose them so that all right hand side terms of $\tilde{\mathbf{t}}^k$ in (3) are zero except for $\mathtt{deg}(\partial^2_{vv}\mathbf{t}^k) = 3$. Then $5 = \mathtt{deg}(\partial_{vv}\tilde{\mathbf{t}}^k) = 2\mathtt{deg}(a^k) + \mathtt{deg}(\partial^2_{vv}\mathbf{t}^k) = 2\mathtt{deg}(a^k)+3$ and $\mathtt{deg}(a^k) \leq 1$ must hold. Setting next all terms $\mathbf{t}^k_{ij} = 0$ for

$j = 0, 2$, the only non-zero right hand side terms of (3) are $\mathsf{deg}((a^k)^2\partial_{vv}^2\mathbf{t}^k) = 5$, $\mathsf{deg}(2a^k b^k \partial_u\partial_v \mathbf{t}^k) = 3 + \mathsf{deg}(b^k) \le 6$ and $\mathsf{deg}(d^k\partial_v\mathbf{t}^k) \le \mathsf{deg}(d^k) + 3$. Therefore $\mathsf{deg}(d^k) \le 3$. Independent choice of the BB-coefficients $\mathbf{t}^k_{i1}$, $i = 0, \ldots, 3$ shows that the degree 6 terms cannot always cancel one another. Therefore, for general input $\mathbf{t}$, $\mathsf{deg}(d^k) \le 2$. Finally, considering all terms not already bounded by degree 5, $\mathsf{deg}((b^k)^2\partial_{uu}^2\mathbf{t}^k) \le 6 + 1$ and $\mathsf{deg}(e^k\partial_u\mathbf{t}^k) \le \mathsf{deg}(e^k) + 2$ implies $\mathsf{deg}(e^k) \le 5$; but again, independent choice of the BB-coefficients $\mathbf{t}^k_{ij}$ shows that neither degree 6 nor degree 7 terms can always cancel one another, so that $\mathsf{deg}(e^k) \le 3$ must hold. |||

Binary splitting the tensor-borders $\mathbf{t}^k$, $\tilde{\mathbf{t}}^k$

$$\mathbf{t}^{k,0}(u,v) := \mathbf{t}^k(\frac{u}{2}, \frac{v}{2}), \quad \mathbf{t}^{k,1}(u,v) := \mathbf{t}^k(\frac{1}{2} + \frac{u}{2}, \frac{v}{2}),$$
$$\tilde{\mathbf{t}}^{k,0}(u,v) := \tilde{\mathbf{t}}^k(\frac{u}{2}, \frac{v}{2}), \quad \tilde{\mathbf{t}}^{k,1}(u,v) := \tilde{\mathbf{t}}^k(\frac{1}{2} + \frac{u}{2}, \frac{v}{2})$$

(Fig. 5 c illustrates the left part of such consecutive splits) implies reparameterizations $\rho^{k,r}$, $r = 0, 1$ with

$$\begin{aligned} a^{k,0}(u) &:= a^k(\frac{u}{2}),\ a^{k,1}(u) := a^k(\frac{1}{2} + \frac{u}{2}), \\ b^{k,0}(u) &:= b^k(\frac{u}{2}),\ b^{k,1}(u) := b^k(\frac{1}{2} + \frac{u}{2}), \\ d^{k,0}(u) &:= \frac{1}{2}d^k(\frac{u}{2}),\ d^{k,1}(u) := \frac{1}{2}d^k(\frac{1}{2} + \frac{u}{2}), \\ e^{k,0}(u) &:= \frac{1}{2}e^k(\frac{u}{2}),\ e^{k,1}(u) := \frac{1}{2}e^k(\frac{1}{2} + \frac{u}{2}). \end{aligned} \tag{5}$$

Lemma 2 (**b, e across $\mathbb{c}$,$\mathbb{m}$**). *Flexibility-increasing refinement of the G^2 bi-5 tensor-border $\tilde{\mathbf{t}}^k$ implies*

$$b_0^k + 2b_1^k + b_2^k = 0 \quad \textit{and } e_0^k + 3e_1^k + 3e_2^k + e_3^k = 0.$$

Proof If the split pieces $\mathbf{t}^{k,0}$ and $\mathbf{t}^{k,1}$ are C^2-connected and reparameterized by (5) then $\tilde{\mathbf{t}}^{k,0}$ and $\tilde{\mathbf{t}}^{k,1}$ must also be C^2-connected. Setting equal the expansions of the second derivative in u

$$\begin{aligned} \partial_{vuu}\tilde{\mathbf{t}}^{k,i} &= \partial_{uu}a^{k,i}\partial_v\mathbf{t}^{k,i} + 2\partial_u a^{k,i}\partial_{uv}\mathbf{t}^{k,i} + a^{k,i}\partial_{vuu}\mathbf{t}^{k,i} \\ &\quad + \partial_{uu}b^{k,i}\partial_u\mathbf{t}^{k,i} + 2\partial_u b^{k,i}\partial_{uu}\mathbf{t}^{k,i} + b^{k,i}\partial_{uuu}\mathbf{t}^{k,i} \end{aligned} \tag{6}$$

of the G^1 constraints $(\partial_v\tilde{\mathbf{t}}^{k,0})(1) = (\partial_v\tilde{\mathbf{t}}^{k,1})(0)$, we observe that (due to C^2 continuity in u of $a^{k,i}$, $b^{k,i}$, $\mathbf{t}^{k,i}$ and $\partial_v\mathbf{t}^{k,i}$) all terms agree except possibly

$$b^{k,0}(1)\partial_{uuu}\mathbf{t}^{k,0}(1) = b^{k,1}(0)\partial_{uuu}\mathbf{t}^{k,1}(0). \tag{7}$$

(7) holds if and only if the boundary curves $\mathbf{t}^{k,0}(u,0)$ and $\mathbf{t}^{k,1}(u,0)$ are C^3-connected – or $b^{k,0}(1) = b^{k,1}(0) = b_0^k + 2b_1^k + b_2^k = 0$. The claim follows since the first option means that the boundary remains a single cubic curve under refinement, i.e. the refinement does not increase flexibility.

Analogously, removing terms that agree due to C^2 continuity and since $b^{k,0}(1) = b^{k,1}(0) = 0$, setting equal the expansions of the second derivative in u of the G^2-constraints $(\partial_{vv}\tilde{\mathbf{t}}^{k,0})(1) = (\partial_{vv}\tilde{\mathbf{t}}^{k,1})(0)$, reduces to $e^{k,0}(1)\partial_{uuu}\mathbf{t}^{k,0} = e^{k,1}(0)\partial_{uuu}\mathbf{t}^{k,0}$ and this forces $\mathbf{t}^{k,0}(u,0)$ and $\mathbf{t}^{k,1}(u,0)$ to be C^3-connected, hence a single polynomial and not flexibility-increasing, or else $e^{k,0}(1) = e^{k,1}(0) = e_0^k + 3e_1^k + 3e_2^k + e_3^k = 0$. |||

Lemma 3 (**a,b,d,e across $\mathbb{c}$,$\mathbb{m}$**). *Flexibility-increasing refinability of the G^2 bi-5 tensor-border $\tilde{\mathbf{t}}^k$ implies that $b^k(u) \equiv 0$ and $e^k(u) \equiv 0$ for all $k = 0, 1, \ldots, N$. Diagonal symmetry additionally implies $a^k(u) \equiv 1$ and $d^k(u) \equiv 0$.*

Proof Applying Lemma 2 to $\tilde{\mathbf{t}}^k$ yields the constraint $b_2^k := -b_0^k - 2b_1^k$, i.e. $b^{k,0} \sim [b_0^k, \frac{b_0^k}{2} + \frac{b_1^k}{2}, 0]$ and $e_3^k := -e_0^k - 3e_1^k - 3e_2^k$ and hence $e^{k,0} \sim [\frac{e_0^k}{2}, \frac{e_0^k}{4} + \frac{e_1^k}{4}, \frac{e_0^k}{8} + \frac{e_1^k}{4} + \frac{e_2^k}{8}, 0]$. We now iterate binary splits and focus on the left pieces as illustrated in Fig. 5 c. Abbreviating

$$\dot{b} := b^{k,0},\ \dot{e} := e^{k,0}, \quad \ddot{b} := \dot{b}^0, \ddot{e} := \dot{e}^0, \dddot{e} := \ddot{e}^0,$$

for the left pieces, the constraints of Lemma 2 imply $\ddot{b} \sim [b_0^k, b_0^k/4, 0]$. Re-applying Lemma 2 to $\ddot{b}$ yields $b_0^k := 0$ and hence $b_1^k = 0 = b_2^k$, i.e. $b^k(u) \equiv 0$. Applying Lemma 2 to $\dot{e}$ and then re-applying twice yields respectively

$$\ddot{e} \sim [e_0^k/4, 3e_0^k/16 + e_1^k/16, 7e_0^k/96 + e_1^k/32, 0],$$
$$\dddot{e} \sim [e_0^k/8, 5e_0^k/96, e_0^k/64, 0], \quad e_0^k := 0.$$

and hence $e_1^k = e_2^k = e_3^k = 0$ as claimed.

Now consider the part of $\tilde{\mathbf{t}}^0$ marked by the left $\square$ in Fig. 1 a. Diagonal symmetry of $\tilde{\mathbf{t}}^0$ implies that $a^0 \equiv 1$ and $d^0 \equiv 0$. By assumption on the internal smoothness of each sector, the tensor-borders $\tilde{\mathbf{t}}^k$ and $\tilde{\mathbf{t}}^{k+1}$ are C^2-connected. Therefore the zeroth, first and second derivative in u (corresponding to the boundary between cap and surrounding surface) of the G^1 constraints $(\partial_v\tilde{\mathbf{t}}^k)(1) = (\partial_v\tilde{\mathbf{t}}^{k+1})(0)$, (see (6)) and $b \equiv 0$ imply that a^k and a^{k+1} are C^2-connected. The analogous argument for the G^2 constraints implies that d^k and d^{k+1} are C^2-connected. Then the claim follows from the degree bounds on a^k and d^k. |||

Corollary 1. *Each $\tilde{\mathbf{t}}^k$ equals $\mathbf{t}^k$ in degree-raised form.*

For the overall theorem we look additionally at the refinement along sector-separating curves.

Theorem 1. *Symmetric, unbiased, multi-sided bi-5 G^2 constructions with internally C^2 sectors can not be refined flexibility-increasing.*

Proof For polynomial pieces $\mathbf{p}^N$, $\vec{\mathbf{p}}^N$ (sector-pieces of degree bi-5) and $\mathbf{t}^N$, $\vec{\mathbf{t}}^N$ (tensor-border of degree bi-3) meating at $\mathbb{m}^s$, Corollary 1 implies $\vec{\mathbf{p}}_{i1}^N := 2\mathbf{p}_{i0}^N - \mathbf{p}_{i1}^N$, $i = 3, 4, 5$ (see the right $\square$ in Fig. 1 a and the indices in Fig. 5 b). Since the sectors are constructed without bias, the G^1 constraints (2) have the form $\partial_v\vec{\mathbf{p}}^N = -\partial_v\mathbf{p}^N + b^N(u)\partial_u\vec{\mathbf{p}}^N$. Consider the choice of least-degree: $b^N(u) := \gamma^N(1-u)^3$ for $\gamma_N \in \mathbb{R}$. The comparison of degrees, $\mathsf{deg}(b^0\partial_u\mathbf{p}) = 3 + \mathsf{deg}(\partial_u\mathbf{p}) = \mathsf{deg}(\partial_v\vec{\mathbf{p}} + \partial_v\mathbf{p}) \le 5$, implies $\mathsf{deg}(\partial_u\mathbf{p}) \le 2$. Hence the piece of sector-separating curve between $\mathbf{p}^N$ and $\vec{\mathbf{p}}^N$ is of actual degree at most 3. Any higher-degree choice of $b^N(u)$ would yield even lower degree and further curtail flexibility.

Refining the sector-pieces $\mathbf{p}^N$ and $\vec{\mathbf{p}}^N$ yields four pieces $\mathbf{p}^{N,0}$, $\mathbf{p}^{N,1}$, $\vec{\mathbf{p}}^{N,0}$, $\vec{\mathbf{p}}^{N,1}$. Calculating derivatives as in (6) yields the analogous equality $b^{N,0}(1)\partial_{uuu}\mathbf{p}^{N,0}(1) = b^{N,1}(0)\partial_{uuu}\mathbf{p}^{N,1}(0)$. If $\partial_{uuu}\mathbf{p}^{N,0}(1) = \partial_{uuu}\mathbf{p}^{N,1}(0)$ then the pieces form a single cubic polynomial, i.e. refinement does not increase flexibility. Otherwise $b^{N,0}(1) = b^{N,1}(0) = \frac{\gamma^N}{8} = 0$ must hold and this implies that $\vec{\mathbf{p}}_{i1}^N := 2\mathbf{p}_{i0}^N - \mathbf{p}_{i1}^N$ for all $i = 0, \ldots, 5$. Since macro-patches are internally C^2, $\vec{\mathbf{p}}_{i1}^{N-1} := 2\mathbf{p}_{i0}^{N-1} - \mathbf{p}_{i1}^{N-1}$, $i = 3, 4, 5$, for the next piece towards $\mathbb{o}$, and flexibility-increasing refinement implies $\gamma^{N-1} = 0$. Proceeding along the sector-separating curve, $\gamma^0 = 0$ conflicts with the n-sided configuration, $n \ne 4$ at $\mathbb{o}$. |||

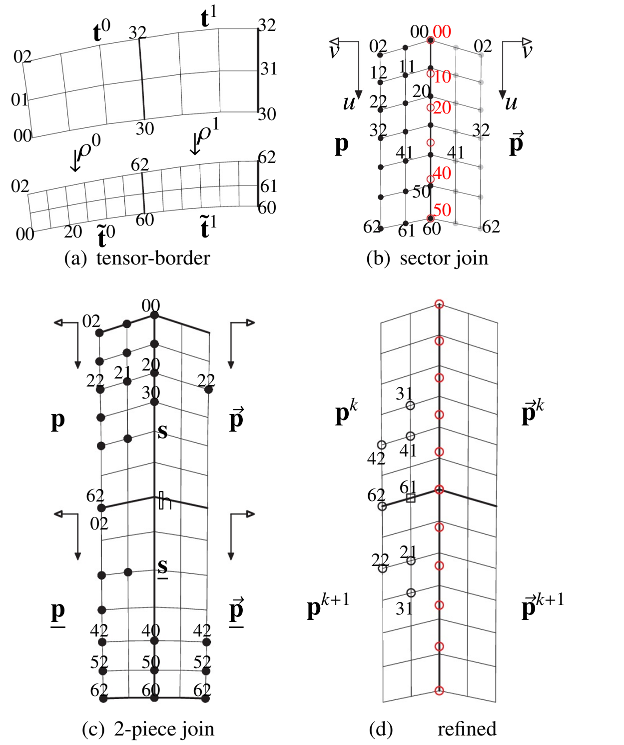

(a) tensor-border (b) sector join (c) 2-piece join (d) refined join

Figure 6: Bi-6 construction: layout and notation for G^2 data. (a) 2-piece tensor-border; (b,c,d) sectors along the sector-separating curve from $\mathbb{o}$ to $\mathbb{m}$. (b) Generic piece: the sector-separating curve is of reduced degree 5. Its BB-coefficients are marked $\circ$. (c) The main construction; (d) Generic pieces k and $k+1$ during refinement. Note that in (a) the u-direction is horizontal, whereas in (b), (c) u corresponds to the full 'down' arrow (while the hollow arrows mark the v-direction).

4. Geometric bi-6 construction

This section defines a multi-sided, symmetric, unbiased G^2 bi-6 surface cap sufficiently flexible for inclusion into any bi-cubic C^2 spline complex. Fig. 1 b showed the layout. Each of the n sectors consists of 2×2 polynomial pieces of degree bi-6 that join C^2; the gray-underlaid strips of BB-coefficients guarantee G^2-continuity both with the input data along $\mathbb{m}^{s-1}, \mathbb{c}, \mathbb{m}^s$ and between the sectors along $\mathbb{o}, \mathbb{m}^s$. The BB-coefficients marked as $\circ$ represent Hermite data up to order 3 at the extraordinary point, namely the *cubic expansion* $\mathbf{c}$ of a map $\tilde{\mathbf{c}}$ of total degree 3, reparameterized. The quality of the surfaces is typically very good, see Fig. 10. Section 5 will prove flexibility-increasing G^2-refinability of this construction by explicitly exposing new free coefficients along the boundary curves and in the interior.

4.1. Specific G^2 constraints

Fig. 6 b shows a generic piece of the cap along a sector-separating curve. For a quadratic $b(u) := \sum_{i=0}^2 b_i B_i^2(u)$ and $d(u) := 0$ the unbiased setup yields $a(u) := -1$, $e(u) := b(u)b'(u)$. Note that we re-use a,b, d, e to name the functions of ρ along the sector-separating curve, $\mathbb{o}, \mathbb{m}^s$ – not to be confused with the a,b, d, e used along the tensor-border $\mathbb{c}^s, \mathbb{m}^s$. The constraint

$$\partial_v \vec{\mathbf{p}} = -\partial_v \mathbf{p} + b(u)\partial_u \mathbf{p} \tag{8}$$

then implies that $\mathbf{s}$ is of degree 5 (see the BB-coefficients marked as $\circ$ in Fig. 6 b). The G^2 constraint (3) now reduces to

$$\partial^2_{vv}\vec{\mathbf{p}} = \partial^2_{vv}\mathbf{p} - 2b(u)\partial_u\partial_v\mathbf{p} + b^2(u)\partial^2_{uu}\mathbf{p} + b(u)b'(u)\partial_u\mathbf{p}\,. \tag{9}$$

For an extraordinary point of valence n, we choose

$$b \sim \mathsf{c}[2,\ 2,\ 1]; \qquad \underline{b} \sim \mathsf{c}[1,0,0]; \quad \mathsf{c} := \cos\frac{2\pi}{n}, \tag{10}$$

where b reparameterizes the piece $\mathbf{s}$ closer to $\mathbb{o}$, and $\underline{b}$ the piece $\underline{\mathbf{s}}$ closer to $\mathbb{m}$, see Fig. 6 c; Section 6 explains the rationale underlying the specific choice.

4.2. Pre-solving G^2 constraints within the cap

C^0 continuity between the sectors follows from $\vec{\mathbf{p}}_{i0} := \mathbf{p}_{i0}$, $\underline{\vec{\mathbf{p}}}_{i0} := \underline{\mathbf{p}}_{i0}$, for $i = 0, 1, \ldots, 6$, and degree 5 of the sector-separating curve is enforced as

$$\sum_{i=0}^{6}(-1)^i\binom{6}{i}\mathbf{p}_{i0} = 0, \quad \sum_{i=0}^{6}(-1)^i\binom{6}{i}\underline{\mathbf{p}}_{i0} = 0. \tag{11}$$

Since the G^1 constraints are of degree 6 and the G^2 constraints of degree 7, they form a system of $7+7+8+8 = 30$ linear equations. Joining C^2 the pieces $\underline{\mathbf{p}}$ and $\mathbf{p}$, respectively $\underline{\vec{\mathbf{p}}}$ and $\vec{\mathbf{p}}$, (with $\underline{\mathbf{p}}, \underline{\vec{\mathbf{p}}}$ closer to $\mathbb{m}$) by setting

$$\begin{aligned}
&\underline{\mathbf{p}}_{0j} := \mathbf{p}_{6,j}, \quad \underline{\vec{\mathbf{p}}}_{0\underline{j}} := \vec{\mathbf{p}}_{6,\underline{j}}, \qquad j = 0,1,2,\ \underline{j} = 1,2,\\
&\mathbf{p}_{5j} := \mathbf{p}_{6j} + \frac{\mathbf{p}_{4j} - \underline{\mathbf{p}}_{2j}}{4}, \quad \underline{\mathbf{p}}_{1j} := \mathbf{p}_{6j} - \frac{\mathbf{p}_{4j} - \underline{\mathbf{p}}_{2j}}{4},\\
&\vec{\mathbf{p}}_{5\underline{j}} := \vec{\mathbf{p}}_{6\underline{j}} + \frac{\vec{\mathbf{p}}_{4\underline{j}} - \underline{\vec{\mathbf{p}}}_{2\underline{j}}}{4}, \quad \underline{\vec{\mathbf{p}}}_{1\underline{j}} := \vec{\mathbf{p}}_{6\underline{j}} - \frac{\vec{\mathbf{p}}_{4\underline{j}} - \underline{\vec{\mathbf{p}}}_{2\underline{j}}}{4};
\end{aligned} \tag{12}$$

and then solving the equations, leaving unconstrained the coefficients marked as $\bullet$ in Fig. 6 c, yields

$$\begin{aligned}
&\underline{\mathbf{p}}_{i1} := \underline{\mathbf{p}}_{i0} + \frac{\underline{\mathbf{p}}_{i2} - \underline{\vec{\mathbf{p}}}_{i2}}{4},\ \underline{\vec{\mathbf{p}}}_{i1} := \underline{\mathbf{p}}_{i0} - \frac{\underline{\mathbf{p}}_{i2} - \underline{\vec{\mathbf{p}}}_{i2}}{4},\ \underline{i} = 5,6;\\
&w_1 := -\frac{b_0}{100},\ w_2 := -w_1,\ w_3 := \frac{b_0}{30},\\
&\underline{\mathbf{p}}_{41} := \underline{\mathbf{p}}_{40} + \frac{1}{4}(\underline{\mathbf{p}}_{42} - \underline{\vec{\mathbf{p}}}_{42}) - w_3(\underline{\mathbf{p}}_{50} - \underline{\mathbf{p}}_{60})\\
&\qquad + w_2(\underline{\mathbf{p}}_{52} - \underline{\vec{\mathbf{p}}}_{52}) + w_1(\underline{\mathbf{p}}_{62} - \underline{\vec{\mathbf{p}}}_{62}),\\
&\underline{\vec{\mathbf{p}}}_{41} := \underline{\mathbf{p}}_{40} - \frac{1}{4}(\underline{\mathbf{p}}_{42} - \underline{\vec{\mathbf{p}}}_{42}) - w_3(\underline{\mathbf{p}}_{50} - \underline{\mathbf{p}}_{60})\\
&\qquad - w_2(\underline{\mathbf{p}}_{52} - \underline{\vec{\mathbf{p}}}_{52}) - w_1(\underline{\mathbf{p}}_{62} - \underline{\vec{\mathbf{p}}}_{62}).
\end{aligned} \tag{13}$$

At $\mathbb{m}$ assignment (13) is consistent with the input tensor-border data after splitting it into two pieces $\mathbf{t}^k$, $k = 0, 1$ (see Fig. 6 a) reparameterized by their respective ρ^k with

$$\begin{aligned}
&a^k(u) := 1,\ b^k(u) := 0,\ e^k(u) := 0,\ k = 0,1, \quad \delta := \frac{d_3^1}{4} - \frac{\mathsf{c}}{12},\\
&d^k(u) := \sum_{i=0}^{3} d_i^k B_i^3(u), \quad d^0 \sim [0,0,0,\delta],\ d^1 \sim [\delta, 2\delta, 4\delta, d_3^1].
\end{aligned}$$

As default we set

$$d_3^{1,def} := \frac{2\mathsf{c}}{3}. \tag{14}$$

Since $\mathbf{p}_{ij}^{s+1} = \vec{\mathbf{p}}_{ji}^s$, for $i + j \le 2$ the coefficients $\mathbf{p}_{ij}^s$ in sectors $s > 0$ can be uniquely expressed in terms of the six quadratic expansion coefficients $\mathbf{p}_{ij}^0$. This is necessary but not sufficient for the solutions across all n sector-separating curves to be consistent at the central point $\mathbb{o}$.

4.3. Construction via a guide surface

To achieve good shape, the cap follows a piecewise C^1 guide surface $\mathbf{g}$ whose construction and tabulation for each valence n is explained in detail in [23]. Other, at first glance natural alternatives intended to optimize shape fail due to the large number of unconstrained coefficients among the 2×2 degree bi-6 pieces per sector. The guide $\mathbf{g}$ is of total degree 6 (see Fig. 7 a). Its center (pink-underlaid BB-coefficients) represents a degree 3 map $\tilde{\mathbf{c}}$ in degree-raised form, see Fig. 7 b. The map is defined by 10 BB-coefficients of one sector, shown as • in Fig. 7 a.

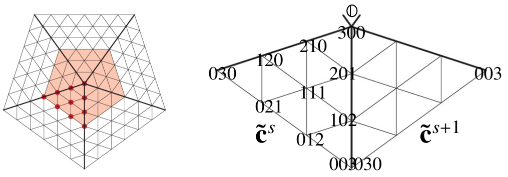

(a) guide $\mathbf{g}$ (b) cubic map $\tilde{\mathbf{c}}$

Figure 7: (a) The $n = 5$ sectors of the guide $\mathbf{g}$, a C^1 map of piecewise total degree 6. The pink-underlaid center is a total degree 3 map $\tilde{\mathbf{c}}$. (c) The BB-coefficients of $\tilde{\mathbf{c}}$.

In each sector s we compose the guide $\mathbf{g}$ with the reparameterization $\tau : \mathbb{R}^2 \to \mathbb{R}^2$ whose layout is that of Fig. 1 b. Then each sector of τ is constructed to be

- G^2-connected to adjacent sectors via the pre-solved constraints of Section 4.2;
- G^2-connected using ρ with the tensor-border of the characteristic ring of Catmull-Clark subdivision [24, Chapter 5];
- internally C^2;
- both diagonally and rotationally symmetric, see Fig. 8 .

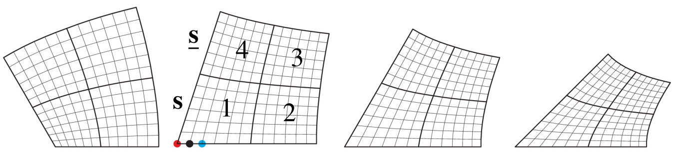

(a) $n = 3$ (b) $n = 5$ (c) $n = 6$ (d) $n = 8$

Figure 8: Reparameterizations τ.

The coefficients of τ unconstrained after enforcing • := $\frac{1}{2}$• + $\frac{1}{2}$• for the coefficients indicated in Fig. 8 b, minimize the functional $\mathcal{F}_3 f := \int_0^1 \int_0^1 \sum_{i+j=3,i,j\geq 0} \frac{3!}{i!j!} (\partial_s^i \partial_t^j f(s,t))^2 \, ds \, dt$, applied to the four pieces of one sector (and hence to all sectors by rotational symmetry).

The following inheritance of smoothness by $\mathbf{g} \circ \tau$ at © (see the BB-coefficients marked ∘ in Fig. 1 b) is checked by inspection.

Lemma 4 (cubic expansion c yields G^2 join at ©). *Let $\mathbf{c}^s_{ij}$, $\mathbf{c}^{s+1}_{ij}$, $i + j \leq 3$ denote the BB-coefficients of the cubic expansions $\mathbf{c}^s$ and $\mathbf{c}^{s+1}$ at © obtained by converting the partial derivatives of $\mathbf{h} := \mathbf{g} \circ \tau$ up to order 3 to bi-6 BB-form:*

$$\begin{pmatrix} \partial_v^3\mathbf{h} & \partial_v^2\mathbf{h} & \partial_v\mathbf{h} & \mathbf{h} \\ \partial_u\partial_v^3\mathbf{h} & \partial_u\partial_v^2\mathbf{h} & \partial_u\partial_v\mathbf{h} & \partial_u\mathbf{h} \\ \partial_u^2\partial_v^3\mathbf{h} & \partial_u^2\partial_v^2\mathbf{h} & \partial_u^2\partial_v\mathbf{h} & \partial_u^2\mathbf{h} \\ \partial_u^3\partial_v^3\mathbf{h} & \partial_u^3\partial_v^2\mathbf{h} & \partial_u^3\partial_v\mathbf{h} & \partial_u^3\mathbf{h} \end{pmatrix} \to \begin{pmatrix} \mathbf{c}^s_{03} & \mathbf{c}^s_{02} & \mathbf{c}^s_{01} & \mathbf{c}^s_{00} \\ \cdot & \mathbf{c}^s_{12} & \mathbf{c}^s_{11} & \mathbf{c}^s_{10} \\ \cdot & \cdot & \mathbf{c}^s_{21} & \mathbf{c}^s_{20} \\ \cdot & \cdot & \cdot & \mathbf{c}^s_{30} \end{pmatrix}, \mathbf{c}^{s+1}_{0i} = \mathbf{c}^s_{i0}, i = 0, \ldots, 3. \tag{15}$$

Then the expansions $\mathbf{c}^s$ and $\mathbf{c}^{s+1}$ depend only on BB-coefficients of the cubic map $\tilde{\mathbf{c}}$ at © and are consistent with the G^1 and G^2 constraints between sectors s and $s + 1$.

In each sector and quadrant $k = 1, 2, 3, 4$ of τ (see the labels in Fig. 8 b) the guide $\mathbf{g}$ is composed with τ and the resulting $\mathbf{h} := \mathbf{g} \circ \tau$ is converted into bi-6 patches $\mathbf{f}$ by collecting in each corner the Hermite data (Fig. 9 a) expressed in BB-form (Fig. 9 b), with averaged BB-coefficients at overlapping locations (Fig. 9 c).

$$\begin{pmatrix} \partial_v^3 f & \partial_u\partial_v^3 f & \partial_u^2\partial_v^3 f & \partial_u^3\partial_v^3 f \\ \partial_v^2 f & \partial_u\partial_v^2 f & \partial_u^2\partial_v^2 f & \partial_u^3\partial_v^2 f \\ \partial_v f & \partial_u\partial_v f & \partial_u^2\partial_v f & \partial_u^3\partial_v f \\ f & \partial_u f & \partial_u^2 f & \partial_u^3 f \end{pmatrix} \to$$

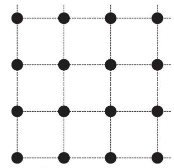

(a) Hermite data (b) BB-form

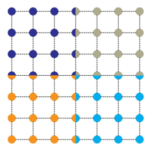

(c) bi-6 patch

Figure 9: (a) Hermite data as partial derivatives converted to (b) BB-form. (c) A patch of degree bi-6 obtained by merging Hermite data at the corners.

4.4. The G^2 cap algorithm

Denote the sets of unconstrained BB-coefficients by $\mathcal{S}_0$ and the set of BB-coefficients of the strip $\mathbf{p}$, $\vec{\mathbf{p}}$, $\underline{\mathbf{p}}$, $\underline{\vec{\mathbf{p}}}$ along a sector-separating curve by $\mathcal{S}$, see Fig. 6 c:

$$\mathcal{S}_0 := \{\mathbf{p}_{32}, \mathbf{p}_{42}, \mathbf{p}_{62}, \mathbf{p}_{41}, \underline{\mathbf{p}}_{22}, \underline{\mathbf{p}}_{32}, \underline{\mathbf{p}}_{21}\},$$
$$\mathcal{S} := \{\mathbf{p}_{32}, \mathbf{p}_{31}, \vec{\mathbf{p}}_{31}, \vec{\mathbf{p}}_{32}; \ldots$$
$$\mathbf{p}_{ij}, \vec{\mathbf{p}}_{ij}, i = 4, 5, 6, j = 0, 1, 2; \; \underline{\mathbf{p}}_{ij}, \underline{\vec{\mathbf{p}}}_{ij}, i = 1, 2, 3, j = 0, 1, 2.\}.$$

Then the bi-6 surface is constructed as follows.

Bi-6 cap construction. Set the BB-coefficients in Fig. 1 b

(i) marked ∘ according to Lemma 4;
(ii) underlaid gray along the curve $\overline{\mathbb{c}, \mathbb{m}}$ as the reparametrized input tensor-border $\tilde{\mathbf{t}}^s$;
(iii) all remaining BB-coefficients of the 2×2 patch in each sector and quadrant as the bi-6 BB-coefficients of $\mathbf{f}$ (the Hermite-sampling of $\mathbf{g} \circ \tau$);
(iv) overwrite $\mathcal{S}$ by minimizing with respect to $\mathcal{S}_0$ the sum of squared distances between the coefficients of $\mathbf{f}$ and $\mathcal{S}$.

The last step ensures G^2 continuity across sector-separating curves. The overall construction can be tabulated and executed as a matrix multiplication.

Fig. 10 displays bi-6 caps for several valencies, assessing the quality, both of the transition from bi-3 surroundings to bi-6 cap and of the cap itself, by highlight lines as well as curvature shadings. The observed monotonicity and uniformity of both measures indicated very high surface quality.

5. Flexibility-increasing G^2-refinability of the bi-6 cap

A uniform binary split via de Casteljau's algorithm refines the bi-6 patches. This section aims to exhibit (all) newly unconstrained BB-coefficients that allow G^2 modifying this trivially

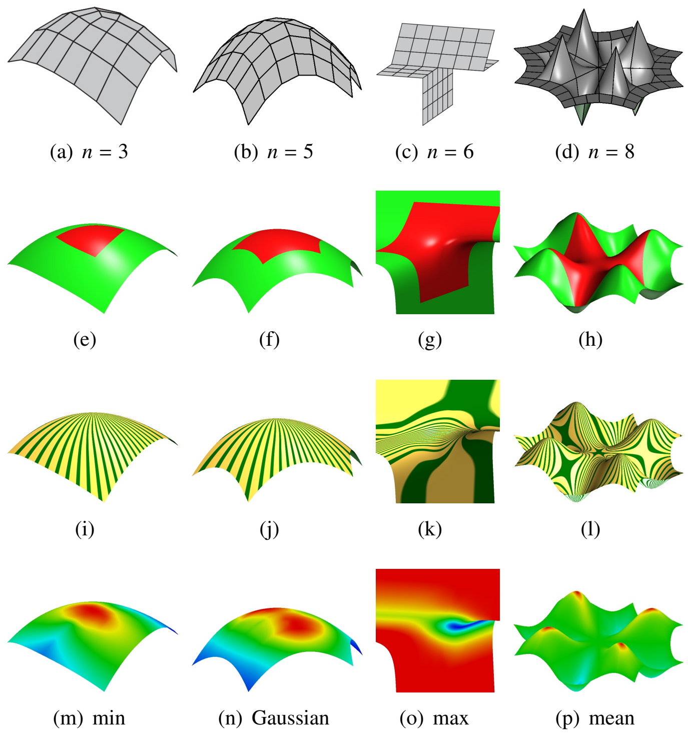

Figure 10: (Top row) Input nets. (Row 2) Layout with bi-3 ring and bi-6 cap. (Row 3) Distribution of highlight lines. (Bottom row) Curvature shading.

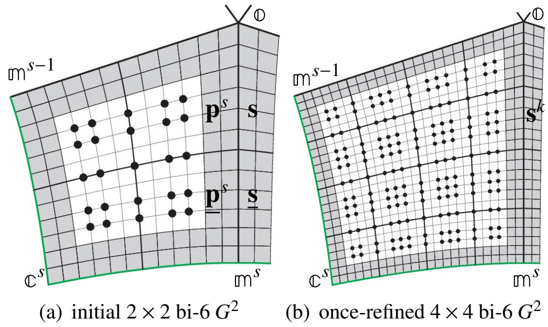

Figure 11: Internal degrees of freedom marked as $\bullet$.

refined surface and so show that the refinement is flexibility-increasing.

In the interior of each sector, flexibility-increasing refinability reduces to uniform knot insertion for a tensor-product bi-6 C^2 spline and needs no further discussion.

Along the boundaries $\mathbb{m}, \mathbb{c}$ the functions $d(u)$ and along $\mathbb{m}, \mathbb{o}$ the functions $b(u)$ are correspondingly split: $d^{ref,0}(u) := d(u/2)$, $d^{ref,1}(u) := d(1/2 + u/2)$ and $b^{ref,0}(u) := b(u/2)$, $b^{ref,1}(u) := b(1/2 + u/2)$. Then, where the refinements along $\mathbb{m}, \mathbb{c}$ and $\mathbb{m}, \mathbb{o}$ overlap near $\mathbb{m}$, the 3×3 groups of BB-coefficients agree. Fig. 14 illustrates the flexibility-increasing G^2-refinement along $\mathbb{m}, \mathbb{c}$: uniform knot insertion refines the green control points of the C^2 bi-cubic spline complex and B-to-BB conversion followed by reparameterization yields the green-underlaid BB-coefficients of bi-6 sector. As B-spline refinements, both interior and outer boundary refinement are then readily seen to be flexibility-increasing.

This section therefore focuses on the (grey-underlaid) strips of BB-coefficients in Fig. 11 that enforce G^2-continuity along sector-separating curves $\mathbb{o}, \mathbb{m}$. A number of technical lemmas, some relegated to the Appendices, are needed to prove and fully characterize the increase in free parameters. First, we consider the generic configuration of Fig. 6. New degrees of freedom in the refined construction are now exhibited by pre-solving the G^2 constraint equations under refinement in terms of these unconstrained coefficients. The key to identifying the unconstrained coefficients is a localizing reformulation of the generic G^2 constraints, i.e. the constraints without consideration of the special interaction with other constraints at $\mathbb{o}$ and $\mathbb{m}$.

5.1. Generic refinement along the sector-separating curves

Recall that the sector-separating curve is of degree 5. Its BB-coefficients $\mathbf{s}_i$, $i = 0, \dots, 5$, are marked as $\circ$ in Fig. 6b. The reparameterization for the G^1 and G^2 constraints (8, 9) are

$$a(u) := -1,\ b(u) := \sum_{i=0}^{2} b_i B_i^2(u),\ d(u) := 0,\ e(u) := b(u)b'(u).$$

We abbreviate the right sides of (8), (9) as

$$\dot{\mathbf{r}}(u) := -\,\partial_v \mathbf{p} + b(u)\partial_u \mathbf{p}\ ,$$
$$\ddot{\mathbf{r}}(u) := \partial_{vv}^2 \mathbf{p} - 2b(u)\partial_u\partial_v \mathbf{p} + b^2(u)\partial_{uu}^2 \mathbf{p} + b(u)b'(u)\partial_u \mathbf{p}\ .$$

Evidently $\mathtt{deg}(\dot{\mathbf{r}}) = 6$ and $\vec{\mathbf{p}}_{i1} := \mathbf{p}_{i,0} + \dot{\mathbf{r}}_i/6$, $i = 0, \dots, 6$. Since $\mathtt{deg}(\ddot{\mathbf{r}}) = 7$ complicates derivation of an explicit solution to the constraints, we reformulate.

Lemma 5 (degree-reducing reformulation). *Define the alternating sums*

$$\hat{b} := \sum_{i=0}^{2}(-1)^i\binom{2}{i}b_i,\ \hat{\mathtt{p}} := \sum_{i=0}^{6}(-1)^i\binom{6}{i}\mathbf{p}_{i1},\ \hat{\mathtt{s}} := \frac{5\hat{b}}{12}\sum_{i=0}^{5}(-1)^i\binom{5}{i}\mathbf{s}_i.$$

Then $\mathtt{deg}(\ddot{\mathbf{r}}(u) + 72\hat{b}(\hat{\mathtt{p}} + \hat{\mathtt{s}})u^7) = 6$.

For $i = 0, \dots, 6$, we denote the BB-coefficients of the reformulation $\ddot{\mathbf{r}}(u) + 72\hat{b}(\hat{\mathtt{p}} + \hat{\mathtt{s}})u^7$ by $\ddot{\mathbf{r}}_i$. Then $\vec{\mathbf{p}}_{i2} := -\mathbf{p}_{i,0} + 2\vec{\mathbf{p}}_{i1} + \ddot{\mathbf{r}}_i/30$. Close examination of the C^2-join of the refined pieces reveals four conditions (1), (2), (3), (4) that when satisfied yields smoothness of the layer curves aligned with the sector boundary.

Lemma 6 (implied smoothness across s). *If*
(1) the alternating sums of coefficients $\hat{\mathtt{p}}^k + \hat{\mathtt{s}}^k = 0 = \hat{\mathtt{p}}^{k+1} + \hat{\mathtt{s}}^{k+1}$ *and the layer curves with coefficients*
(2) $\mathbf{s}_i^k$ *and* $\mathbf{s}_i^{k+1}$, $i = 0, \dots, 5$, *are* C^4*-connected;*
(3) $\mathbf{p}_{i1}^k$ *and* $\mathbf{p}_{i1}^{k+1}$, $i = 0, \dots, 6$, *are* C^3*-connected;*
(4) $\mathbf{p}_{i2}^k$ *and* $\mathbf{p}_{i2}^{k+1}$, $i = 0, \dots, 6$, *are* C^2*-connected*
then the layer curves
(3)* $\vec{\mathbf{p}}_{i1}^k$ *and* $\vec{\mathbf{p}}_{i1}^{k+1}$, $i = 0, \dots, 6$, *are* C^3*-connected;*
(4)* $\vec{\mathbf{p}}_{i2}^k$ *and* $\vec{\mathbf{p}}_{i2}^{k+1}$, $i = 0, \dots, 6$, *are* C^2*-connected.*

Remarkably, (1–4) are not only sufficient but necessary for flexibility-increasing G^2-refinability of unbiased constructions and the C^3 continuity in (3*) then comes for free.

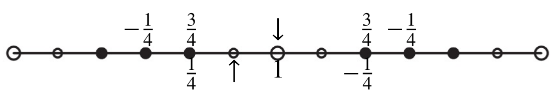

Figure 12: BB-form of a C^3 spline of degree 6 (triple knots).

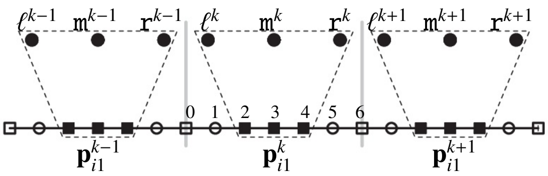

Figure 13: A localized construction of a C^3 spline of degree 6.

Constraints (2), (3) and (4) of Lemma 6 prescribe continuity of the layer curves aligned with sector-separating curves. Combining (1) with (2), (3) and (4), however, makes the computation non-local. To localize the computation of (1–4) we observe that the BB-form of (3) is, cf. Fig. 12 ,

$$\begin{aligned}
&\mathbf{p}^k_{61} := -\frac{1}{4}(\mathbf{p}^k_{31} + \mathbf{p}^{k+1}_{31}) + \frac{3}{4}(\mathbf{p}^k_{41} + \mathbf{p}^{k+1}_{21}),\ \mathbf{p}^{k+1}_{01} := \mathbf{p}^k_{61}\ ;\\
&\mathbf{p}^k_{51} := \mathbf{p}^k_{61} + \frac{1}{4}(\mathbf{p}^k_{41} - \mathbf{p}^{k+1}_{21})\ ,\ \mathbf{p}^{k+1}_{11} := \mathbf{p}^k_{61} - \frac{1}{4}(\mathbf{p}^k_{41} - \mathbf{p}^{k+1}_{21})\ .
\end{aligned} \tag{16}$$

Substituting (16) and the change of variables (see Fig. 13)

$$\begin{aligned}
\mathbf{p}^k_{21} &:= \frac{29\ell^k - 6\mathtt{m}^k + 13\mathtt{r}^k}{36},\ \mathbf{p}^k_{31} := \frac{13\ell^k - 6\mathtt{m}^k + 13\mathtt{r}^k}{20},\\
\mathbf{p}^k_{41} &:= \frac{13\ell^k - 6\mathtt{m}^k + 29\mathtt{r}^k}{36},
\end{aligned} \tag{17}$$

localizes constraint (1) of Lemma 6 as

$$-\mathtt{r}^{k-1} + 2\mathtt{m}^k - \ell^{k+1} + \hat{\mathtt{s}}^k = 0\ . \tag{18}$$

That is,
- ℓ^k and $\mathtt{r}^k$ are unconstrained control points; they prove that the refinement is flexibility-increasing along generic parts of each sector-separating curve ;
- $\mathtt{m}^k$ are calculated from (18); and
- the BB-coefficients $\mathbf{p}^k_{i1}$ are defined by (16) and (17).

5.2. *Smoothness at new splits along the sector-separating curves*

We now split the kth segment along $\mathbb{c}$,$\mathbb{m}$ into a part closer to $\mathbb{c}$ and, indicated by an underline, a part closer to $\mathbb{m}$. Due to C^2 smoothness, after refinement,

$$b^{k+1} \sim [b^k_2, 2b^k_2 - b^k_1, 4b^k_2 - 4b^k_1 + b^k_0];$$

and at the at the midpoint between $\mathbb{c}$ and $\mathbb{m}$ where pieces join C^2 in the original construction

$$\underline{b} \sim [b_2 := \mathtt{c},\ 2b_2 - b_1,\ 2b_2 - b_0]. \tag{19}$$

The following solution takes special consideration of the midpoint $\mathbb{t}^s$.

Lemma 7 (**C^2 along the sector-separating curve).** *If the sector-separating curves with coefficients $\mathbf{s}_i$ and $\underline{\mathbf{s}}_i$, $i = 0,\dots,5$, are C^2-connected, and the layer curves with coefficients $\mathbf{p}_{ij}$ and $\underline{\mathbf{p}}_{ij}$, $i = 0,\dots,6$ are C^2-connected for $j = 1,2$, and if (omitting the superscript ^{ref} throughout in* (20)*, e.g. $b_i := b^{ref}_i$)*

$$\begin{aligned}
v_0 &:= \frac{35\mathtt{c} - b_0 + 2b_1}{48\mathtt{c}},\ v_1 := \frac{59\mathtt{c} - b_0 + 2b_1}{80\mathtt{c}},\\
v_2 &:= \frac{-b_0^2 + 7b_0b_1 - 10b_1^2 - 64\mathtt{c}^2 + 7\mathtt{c}b_0 - 11\mathtt{c}b_1}{864\mathtt{c}},\\
\mathbf{s}_5 &:= -\frac{\mathbf{s}_2 + \underline{\mathbf{s}}_3}{4} + v_0\mathbf{s}_3 + (\frac{3}{2} - v_0)\underline{\mathbf{s}}_2,\\
\mathbf{p}_{61} &:= -\frac{\mathbf{p}_{31} + \underline{\mathbf{p}}_{31}}{4} + v_1\mathbf{p}_{41} + (\frac{3}{2} - v_1)\underline{\mathbf{p}}_{21} - \frac{\mathtt{c}}{48}\mathbf{s}_1\\
&\quad + \frac{5\mathtt{c} + 2b_1 - b_0}{72}\mathbf{s}_2 + v_2\mathbf{s}_3 + (\frac{\mathtt{c} + b_0 - 2b_1}{36} - v_2)\underline{\mathbf{s}}_2\\
&\quad - \frac{7\mathtt{c} - 2b_1 + b_2}{72}\underline{\mathbf{s}}_3 + \frac{\mathtt{c}}{48}\underline{\mathbf{s}}_4\ ,
\end{aligned} \tag{20}$$

then the layer curves $\vec{\mathbf{p}}_{ij}$ and $\underline{\vec{\mathbf{p}}}_{ij}$, $i = 0,\dots,6$ are C^2-connected for $j = 1,2$.

Refinement of the cubic expansion $\mathbf{c}$ *at the extraordinary point* $\mathbb{c}$. To refine at $\mathbb{c}$, the solution provided via reformulation (see Lemma 5) is re-arranged to make the BB-coefficients $\mathbf{p}^{ref}_{ij}$, $0 \le i,j \le 2$ and $\mathbf{p}^{ref}_{30}$ and $\vec{\mathbf{p}}^{ref}_{22}$ are unconstrained (see top markers in Fig. 6 c). Then (15) of Lemma 4 can be applied as for the geometric construction in Section 4. The refinement decomposes into refining the cubic map $\tilde{\mathbf{c}}$ and splitting the part of the reparameterization τ^1 (nearest the origin) of Section 4. The details are given in Appendix A.

Refinement of the sector-separating curves. The refinement is easy after converting the BB-coefficients to independent B-spline coefficients: of a C^4 spline of degree 5 for the sector-separating curve, and of a C^3 spline of degree 6 for the layers of the G^2 strip straddling the sector-separating curve. The details of the conversion are given in Appendix B.

5.3. *Linear independence*

Consider one coordinate, say x, set to 1 the value x^α of one unconstrained control point with index α and to zero all other unconstrained control points, and then apply the bi-6 cap construction. This yields a collection of polynomial pieces in BB-form that we denote g^α.

Recall from the construction that the unconstrained control points fall into four distinct groups, see Fig. 14 .

(a) Control points of the surrounding bicubic spline;
(b) Internal C^2-spline coefficients (●)
(c) Ten control points of the cubic map $\tilde{\mathbf{c}}$ at $\mathbb{c}$;
(d) By Lemma 6 (4) the BB-coefficients $\mathbf{p}_{02}$, $\mathbf{p}_{22}$, $\mathbf{p}_{32}$, $\mathbf{p}_{62}$, $\mathbf{p}_{62}$ can be independently chosen and the localizing reformulation identifies ℓ, $\mathtt{r}$ and $\mathbf{d}$ (see (25) of Appendix B) as control points that can be set freely and define the BB-coefficients marked as ∘ in Fig. 14 . Group (d) consists of the subset of these points that are not used in defining the BB-coefficients marked in Fig. 14 as green-underlaid or ∘.

Proposition 2. *The functions g^α are linearly independent.*

Proof Assume that a linear combination $\sum_\alpha x_\alpha g^\alpha$, of the g^α in the four groups, is the zero function, i.e. all BB-coefficients of the resulting cap are zero. We show that then all x_α must be zero.

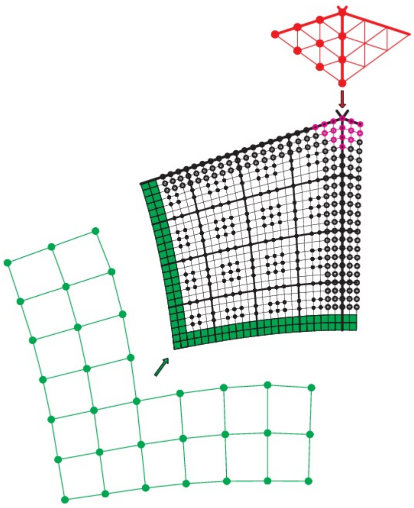

Figure 14: The control point groups of the refined bi-6 G^2 surface.

(a) None of the BB-coefficients of the tensor-border $\mathbf{t}^k$ are set by groups (b),(c),(d). Since the BB-coefficients are obtained by B-to-BB-conversion followed by reparameterization, and the B-splines are linearly independent, $x_\alpha = 0$ for α in group (a).
(b) By definition, the each g^α in group (b) has exactly one non-zero BB-coefficient marked as •. Since all these BB-coefficients are zero, x_α in (b) must be zero.
(c) The derivatives up to degree 3, evaluated at the ⊕-corner of the bi-6 patch, vanish if an only if the 10 control points • of $\mathbf{c}$ vanish, i.e. $x_\alpha = 0$ for α from group (c).
(d) Since the α within group (d) were chosen so that their g^α are linearly independent, all $x_\alpha = 0$.

|||

6. Discussion

The choice of the functions $b(u)$, $\underline{b}(u)$ when reparameterizing along the sector-separating curves (Section 4) is motivated by the desire to have a single formula apply to all irregular valencies. For $n > 4$, b_1 is formally unrestricted, but for $n = 3$ a unique quadratic expansion at center requires $b_1 := 2\mathsf{c} = -1$ and this choice does not harm the surface quality for $n > 4$.

An alternative permissible reparameterization is

$$\rho^k := (u + \frac{1}{2}e^k(u)v^2, v + \frac{1}{2}d^k(u)v^2), k = 0, 1,$$

$$d^0 \sim [0, 0, \frac{\mathsf{c}}{4}], \quad e^0 \sim [0, 0, \frac{\mathsf{c}}{12}, \frac{7\mathsf{c}}{72}], \quad e^1_3 := 0$$

where d^0 and d^1 join C^2; and e^0 and e^1 join C^2. Here we need as input a reparameterized C^3-connected tensor-border of degree 4 to yield a C^2 surface of degree 6 as opposed to our current setting of C^2-connected input data of degree (bi-)3. An increased number of free parameters allows G^2 capping of a sequence of C^2 guided rings as in [25]. Standard (iso-geometric) engineering analysis can then be applied on the regular C^2-joined rapidly contracting C^2 spline rings, see e.g. [23], and a tiny G^2 bi-6 cap that need not be refined. On the downside, the more complex ρ complicates G^2 refinement of the input tensor-border that must be degree-raised to 4 and subsequently C^3-refined, and the increased number of free parameters increases the potential for poor shape.

The general formulas of Section 5 could have also been used in Section 4. However we prefer the approach in Section 4 as it emphasizes the geometric flavor of the construction.

Flexibility-increasing refinability is intended for engineering analysis. Using the extra degrees of freedom naively, either individually or in small groups for geometric manipulation is not effective. This parallels the assessment for G^1 refinement in [26]. For example, in Fig. 15 a the cubic expansion $\mathbf{c}$ is moved up *left* and used to fix unconstrained BB-coefficients as in Section 4. The resulting surface *right*, although G^2, is not well-shaped: the dimples, see Fig. 15 , surely, are not wanted by a designer. In Fig. 15 b, perturbing degrees of freedom across the sector-separating curve *left* yields extended perturbations. Only perturbations interior to a C^2 sector as in (c) produces a predictable outcome.

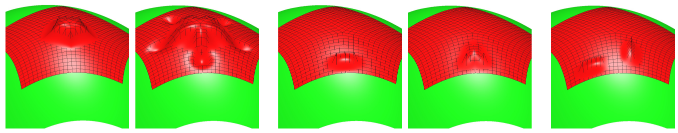

(a) $\mathbf{c}$ shifted up: C^0, G^2 (b) perturbation and smoothing (c) in sector

Figure 15: Individual or groups of degrees of freedom used naively are not suitable for modeling geometric detail – unless they stay within one sector.

A special, different class of irregular points appear in polar layouts. Here the least-degree, general-purpose, polar C^2 constructions [27, 28] are bi-6 and are refinable, since, at the pole, the refinement is based on refining a quadratic expansion analogous to cubic expansion used here.

7. Conclusion

Establishing tight lower degree bounds is hard since one needs to rule out all possible approaches of lesser degree. This paper proved that, for multi-sided configurations within a C^2 spline complex, refinement of G^2 surface constructions with C^2 sectors of degree bi-5 can not generate the expected additional degrees of freedom along the boundaries.

Conversely the paper exhibits a refinable, multi-sided G^2 construction of degree bi-6 (a minimal upper bound) with typically excellent highlight lines. Moreover, all possible degrees of freedom under refinement are characterized. The characterization is technically complex and requires intelligent reformulations to localize the computations. The characterization of the full space proves that the refined construction is flexibility-increasing.

While not useful as direct geometric shape handles the refined constructions can serve for engineering analysis after the geometry is established with the original algorithm. It remains to be seen whether a subspace of the constructions can both serve for engineering applications and provide good geometric shape handles.

Acknowledgements. This work was supported in part by DARPA HR00111720031 and NIH R01 EB018625.

References

[1] A. Collin, G. Sangalli, T. Takacs, Analysis-suitable G^1 multi-patch parametrizations for C^1 isogeometric spaces, Computer Aided Geometric Design 47 (2016) 93–113.
[2] J. Peters, J. Fan, On the complexity of smooth spline surfaces from quad meshes, Computer Aided Geometric Design 27 (2009) 96–105.

[3] K. Karčiauskas, J. Peters, Refinable bi-quartics for design and analysis, Computer-Aided Design (2018) 1–10.
[4] V. Braibant, C. Fleury, Shape optimal design using B-splines, CMAME 44 (1984) 247–267.
[5] Y. Shyy, C. Fleury, K. Izadpanah, Shape optimal design using higher-order elements, CMAME 71 (1988) 99–116.
[6] F. Au, Y. Cheung, Spline finite elements for beam and plate, Computers & Structures 37 (1990) 717–729.
[7] F. Au, Y. Cheung, Isoparametric spline finite strip for plane structures, Computers & Structures 48 (1993) 22–32.
[8] U. Schramm, W. D. Pilkey, The coupling of geometric descriptions and finite elements using NURBS - a study in shape optimization, Finite elements in Analysis and Design 340 (1993) 11–34.
[9] T. J. R. Hughes, J. A. Cottrell, Y. Bazilevs, Isogeometric analysis: CAD, finite elements, NURBS, exact geometry and mesh refinement, Computer Methods in Applied Mechanics and Engineering 194 (2005) 4135–4195.
[10] F. Cirak, M. Scott, E. K. Antonsson, M. Ortiz, P. Schröder, Integrated modeling, finite-element analysis, and engineering design for thin-shell structures using subdivision, Computer-Aided Design 34 (2) (2002) 137–148.
[11] P. J. Barendrecht, Isogeometric analysis for subdivision surfaces, Master's thesis, Technical University of Eindhoven (2013).
[12] T. Nguyen, K. Karčiauskas, J. Peters, A comparative study of several classical, discrete differential and isogeometric methods for solving Poisson's equation on the disk, Axioms 3 (2) (2014) 280–299.
[13] K. Karčiauskas, T. Nguyen, J. Peters, Generalizing bicubic splines for modelling and IGA with irregular layout, Computer Aided Design 70 (2016) 23–35.
[14] M. Kapl, F. Buchegger, M. Bercovier, B. Jüttler, Isogeometric analysis with geometrically continuous functions on planar multi-patch geometries, Computer Methods in Applied Mechanics and Engineering 316 (2017) 209–234.
[15] M. Kapl, V. Vitrih, Space of C^2-smooth geometrically continuous isogeometric functions on two-patch geometries, Computers & Mathematics with Applications 73 (1).
[16] D. Groisser, J. Peters, Matched G^k-constructions always yield C^k-continuous isogeometric elements, Computer Aided Geometric Design 34 (2015) 67–72.
[17] C. T. Loop, S. Schaefer, G ^{2} tensor product splines over extraordinary vertices, Comput. Graph. Forum 27 (5) (2008) 1373–1382.
[18] K. Karčiauskas, J. Peters, Minimal bi-6 G^2 completion of bicubic spline surfaces, Computer Aided Geometric Design 41 (2016) 10–22.
[19] H. Prautzsch, Freeform splines, Comput. Aided Geom. Des 14 (3).
[20] U. Reif, A refineable space of smooth spline surfaces of arbitrary topological genus, Journal of Approximation Theory 90 (2) (1997) 174 – 199.
[21] G. Farin, Curves and Surfaces for Computer Aided Geometric Design: A Practical Guide, Academic Press, 1988.
[22] C. de Boor, A Practical Guide to Splines, Springer, 1978.
[23] K. Karčiauskas, J. Peters, Rapidly contracting subdivision yields finite, effectively C^2 surfaces, Computers & Graphics (2018) 1–10.
[24] J. Peters, U. Reif, Subdivision Surfaces, Vol. 3 of Geometry and Computing, Springer-Verlag, New York, 2008.
[25] K. Karčiauskas, J. Peters, Fair free-form surfaces that are almost everywhere parametrically C^2, Journal of Computational and Applied Mathematics (2018) 1–10.
[26] K. Karčiauskas, J. Peters, Refinable G^1 functions on G^1 free-form surfaces, Computer Aided Geometric Design 54 (2017) 61–73.
[27] K. Karčiauskas, J. Peters, Finite curvature continuous polar patchworks, in: E. Hancock, R. Martin, M. Sabin (Eds.), IMA Mathematics of Surfaces XIII Conference, 2009, pp. 222–234. `doi:10.1007/978-3-642-03596-8_12`.
[28] D. Toshniwal, H. Speleers, R. Hiemstra, T. Hughes, Multi-degree smooth polar splines: A framework for geometric modeling and isogeometric analysis, Computer Methods in Applied Mechanics and Engineering 316 (2017) 1005–1061.

Appendix A: Refinement of $\tilde{\mathbf{c}}$ and τ^1

Fig. 16 illustrates the refinement of the cubic map $\tilde{\mathbf{c}}$ in BB-form. First de Casteljau's algorithm is applied in the direction of the thick layers Fig. 16 a, then in the vertical direction Fig. 16 b to obtain Fig. 16 c. The refinement and conversion to BB-form of degree bi-6 form can be tabulated. With the indices of $\tilde{\mathbf{c}}$ in Fig. 7 b refinement becomes a single matrix multiplication:

$$\tilde{\mathbf{c}}^{ref} := A\tilde{\mathbf{c}} := \frac{1}{8}\begin{pmatrix} 8&0&0&0&0&0&0&0&0&0\\ 4&4&0&0&0&0&0&0&0&0\\ 2&4&2&0&0&0&0&0&0&0\\ 1&3&3&1&0&0&0&0&0&0\\ 4&0&0&0&4&0&0&0&0&0\\ 2&2&0&0&2&2&0&0&0&0\\ 1&2&1&0&1&2&1&0&0&0\\ 2&0&0&0&4&0&0&2&0&0\\ 1&1&0&0&2&2&0&1&1&0\\ 1&0&0&0&3&0&0&3&0&1 \end{pmatrix}\begin{pmatrix} \mathbf{c}_{300}\\ \mathbf{c}_{210}\\ \mathbf{c}_{120}\\ \mathbf{c}_{030}\\ \mathbf{c}_{201}\\ \mathbf{c}_{111}\\ \mathbf{c}_{021}\\ \mathbf{c}_{102}\\ \mathbf{c}_{012}\\ \mathbf{c}_{003} \end{pmatrix}.$$

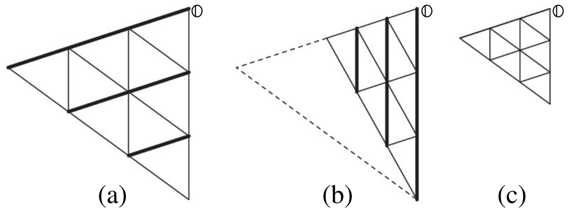

Figure 16: Refinement of the cubic expansion $\mathbf{c}$ at the central point $\circledcirc$ by applying de Casteljau's algorithm.

The BB-coefficients of the cubic expansion $\mathbf{c}$ (red underlaid in Fig. 7 a) are obtained by sampling the cubic expansion of the guide $\mathbf{g}$ (see $\circ$ points in Fig. 1 b) with τ^1. Degree-raised to 6, $\mathbf{c}$ has the same same domain as $\mathbf{g}$ (see Fig. 7 b).

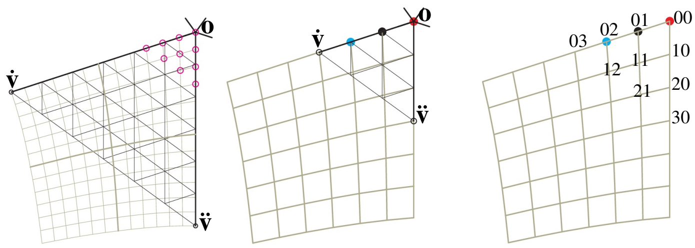

(a) sampling $\mathbf{g}$ with τ (b) domain of $\mathbf{c}$ (c) indices of τ

Figure 17: (a) Sampling the guide $\mathbf{g}$ with τ. The domain of the guide is a sector of a regular unit n-gon spanned by $\mathbf{o} := (0, 0)$, $\dot{\mathbf{v}}$,$\ddot{\mathbf{v}}$ (see Fig. 7 a). The BB-coefficients of τ^1 that used in determining $\mathbf{c}$ in (15) are marked $\circ$. (b,c) The relevant part of τ when sampling $\circledcirc$: $\bullet := \tau_{00}$, $\bullet := \tau_{01}$, $\bullet := \tau_{02}$.

We reformulate and scale τ^1 so that (see Fig. 17)

$$\bullet := \frac{2}{3}\bullet + \frac{1}{3}\dot{\mathbf{v}},\quad \bullet := \frac{1}{3}\bullet + \frac{2}{3}\dot{\mathbf{v}}. \tag{21}$$

The result , denoted τ, has explicit BB-coefficients

$$\begin{pmatrix}\tau_{00}\\ \tau_{01}\\ \tau_{02}\\ \tau_{10}\\ \tau_{20}\end{pmatrix} := \frac{1}{3}\begin{pmatrix}0&0&1\\1&0&2\\2&0&1\\0&1&2\\0&2&1\end{pmatrix}\begin{pmatrix}\dot{\mathbf{v}}\\ \ddot{\mathbf{v}}\\ \mathbf{o}\end{pmatrix},$$

$$\begin{pmatrix}\tau_{03}\\ \tau_{30}\\ \tau_{11}\\ \tau_{12}\\ \tau_{21}\end{pmatrix} := \begin{pmatrix}\mu_0&0&1-\mu_0\\ 0&\mu_0&1-\mu_0\\ \mu_1&\mu_1&1-2\mu_1\\ \mu_2&\mu_3&1-\mu_2-\mu_3\\ \mu_3&\mu_2&1-\mu_2-\mu_3\end{pmatrix}\begin{pmatrix}\dot{\mathbf{v}}\\ \ddot{\mathbf{v}}\\ \mathbf{o}\end{pmatrix} \tag{22}$$

where, for $n = 3, 5, 6, \ldots, 10$, $\mu_0 := 1 + \kappa_n/10^5$,

$$\begin{aligned}&\kappa_n := 185,\ 1033,\ 352,\ -145,\ -469,\ -687,\ -840,\\ &\mu_1 := \frac{1}{3}, \mu_2 := \frac{2}{3} - \frac{61c}{135} + \frac{4c\mu_0}{9},\ \mu_3 := \frac{29}{270} + \frac{2\mu_0}{9}.\end{aligned} \tag{23}$$

The BB-coefficients used in the composition in the refinement are defined as $\tau^{ref}_{ij} := 2\tilde\tau_{i,j}$, $0 \le i + j \le 3$, where $\tilde\tau := \tau(\frac{u}{2}, \frac{v}{2})$. This preserves (21) and τ^{ref}_{ij} is obtained from (22) with

$$\mu^{ref}_0 := \frac{3+\mu_0}{4},\ \mu^{ref}_1 := \frac{1+3\mu_1}{6},$$
$$\mu^{ref}_2 := \frac{4+6\mu_1+3\mu_2}{12},\ \mu^{ref}_3 := \frac{1+6\mu_1+3\mu_3}{12}$$

and $\tilde\tau := A\tau$ where the ten indices of τ according to Fig. 17 b are

$$00, 01, 02, 03, 10, 11, 12, 20, 21, 30. \tag{24}$$

Analogously, after scaling $\mathbf{c}(\frac{u}{2}, \frac{v}{2})$ towards the origin $\mathbf{o}$, one obtains $\mathbf{c}^{ref}$, see Fig. 16 . The explicit formulas allow verification of the following decomposition.

Proposition 3 (decomposition of composed refinement). *For the cubic expansions*

$$(\mathbf{c}\circ\tau)^{ref} := (\mathbf{c}\circ\tau)(\frac{u}{2}, \frac{v}{2}) = \mathbf{c}^{ref}\circ\tau^{ref}.$$

Mapping indices as in (24), ten BB-coefficients $\mathbf{p}^{\mathbb{o}}$ of the (refined) output patch $\mathbf{p}$ are obtained from the (refined) expansion $\mathbf{c}$ via $\mathbf{p}^{\mathbb{o}} := B\mathbf{c}$, where $B :=$

$$\begin{pmatrix}
1 & 0 & 0 & 0 & 0 & 0 & 0 & 0 & 0 & 0\\
0 & 1 & 0 & 0 & 0 & 0 & 0 & 0 & 0 & 0\\
\frac{-1}{5} & \frac{2}{5} & \frac{4}{5} & 0 & 0 & 0 & 0 & 0 & 0 & 0\\
3(1-\mu_0) & 3\mu_0-\frac{18}{5} & \frac{6}{5} & \frac{2}{5} & 0 & 0 & 0 & 0 & 0 & 0\\
0 & 0 & 0 & 0 & 1 & 0 & 0 & 0 & 0 & 0\\
\frac{5}{3}-6\mu_1 & 3\mu_1-\frac{2}{3} & 0 & 0 & 3\mu_1-\frac{2}{3} & \frac{2}{3} & 0 & 0 & 0 & 0\\
\frac{48\mu_1}{5}-3(\mu_2+\mu_3)-\frac{1}{3} & \frac{12}{5}-\frac{72\mu_1}{5}+3\mu_2 & \frac{24\mu_1}{5}-\frac{16}{15} & 0 & \frac{8}{15}-\frac{24\mu_1}{5}+3\mu_3 & \frac{24\mu_1}{5}-\frac{4}{5} & \frac{4}{15} & 0 & 0 & 0\\
\frac{-1}{5} & 0 & 0 & 0 & \frac{2}{5} & 0 & 0 & \frac{4}{5} & 0 & 0\\
\frac{48\mu_1}{5}-3(\mu_2+\mu_3)-\frac{1}{3} & \frac{8}{15}-\frac{24\mu_1}{5}+3\mu_3 & 0 & 0 & \frac{12}{5}-\frac{72\mu_1}{5}+3\mu_2 & \frac{24\mu_1}{5}-\frac{4}{5} & 0 & \frac{24\mu_1}{5}-\frac{16}{15} & \frac{4}{15} & 0\\
3(1-\mu_0) & 0 & 0 & 0 & 3\mu_0-\frac{18}{5} & 0 & 0 & \frac{6}{5} & 0 & \frac{2}{5}
\end{pmatrix}.$$

Appendix B. Conversion to B-spline form along the sector-separating curves

Since we focus on one sector at a time, we omit the sector index s. We first consider the sector-separating curves, C^4 splines of degree 5 and then the layer curves 'parallel' to the sector-separating curves that are (localized) C^3 splines of degree 6.

Refinement of the sector-separating curve. With the notation of Fig. 18 , i.e. $\mathbf{b}_0 := \mathbb{o}$ the BB-coefficients $\mathbf{b}_i$, $i = 0, \ldots, 3$ are defined by $\mathbf{c}$. (25) expresses the control points $\mathbf{d}^i$, $i = 0, \ldots, 3$ in terms of $\mathbf{b}_i$, $i = 0, \ldots, 3$ and $\mathbf{d}^4$ by inverting the conversion from B- to BB-form given by

$$\begin{pmatrix}\mathbf{b}^s_0\\ \mathbf{b}^s_1\\ \mathbf{b}^s_2\\ \mathbf{b}^s_3\\ \mathbf{b}^s_4\\ \mathbf{b}^s_5\end{pmatrix} := M\mathbf{d} := \frac{1}{120}\begin{pmatrix}1 & 26 & 66 & 26 & 1 & 0\\ 0 & 16 & 66 & 36 & 2 & 0\\ 0 & 8 & 60 & 48 & 4 & 0\\ 0 & 4 & 48 & 60 & 8 & 0\\ 0 & 2 & 36 & 66 & 16 & 0\\ 0 & 1 & 26 & 66 & 26 & 1\end{pmatrix}\begin{pmatrix}\mathbf{d}^s\\ \mathbf{d}^{s+1}\\ \mathbf{d}^{s+2}\\ \mathbf{d}^{s+3}\\ \mathbf{d}^{s+4}\\ \mathbf{d}^{s+5}\end{pmatrix}. \tag{25}$$

Fig. 18 shows the B-spline coefficients (*top*) and the BB-coefficients of a piece (*bottom*) of a C^4 degree 5 spline. The B-spline coefficients $\mathbf{d}^k$ for $k \ge 4$ are then unconstrained. At $\mathbb{m}$, the BB-coefficients $\mathbf{b}_i$, $i = 3, \ldots, 5$ are defined by the reparameterized input data $\mathbf{t}$. (25) expresses the control points $\mathbf{d}^i$, $i = 3, \ldots, 5$ in terms of $\mathbf{d}^1$, $\mathbf{d}^2$ and $\mathbf{b}_i$, $i = 3, \ldots, 5$; $\mathbf{d}^k$ for $k \ge 2$ are then unconstrained. Away from $\mathbb{o}$ and $\mathbb{m}$, mimicking the notation of (20), the BB-coefficients $\mathbf{s}_2$, $\mathbf{s}_3$, $\underline{\mathbf{s}}_2$, $\underline{\mathbf{s}}_3$ are independent

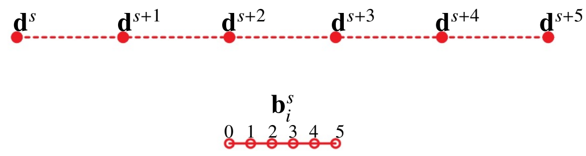

Figure 18: B-spline coefficients of degree 5 C^4 spline and its BB-coefficients.

and define C^2-joined pieces just as at $\mathbb{o}$ but for two formally not interacting groups $\mathbf{d}^i$ and $\underline{\mathbf{d}}^i$, $i = 0, \ldots, 5$. (As before, the part closer to $\mathbb{o}$ caries no super or subscript and the part closer to $\mathbb{m}$ is identified by an underline.) We express the control points $\mathbf{d}^i$, $i = 2, \ldots, 5$ in terms of $\mathbf{d}^1$ and $\mathbf{b}_i$, $i = 2, \ldots, 5$; and the control points $\underline{\mathbf{d}}^i$, $i = 0, \ldots, 3$ in terms of $\underline{\mathbf{d}}^4$ and $\underline{\mathbf{b}}_i$, $i = 0, \ldots, 3$. The new independent BB-coefficients for a flexibility-increasing refinement therefore are

$$\mathbf{b}_2, \mathbf{b}_3, \mathbf{d}^1, \ldots, \quad \underline{\mathbf{b}}_2, \underline{\mathbf{b}}_3, \underline{\mathbf{d}}^4, \ldots$$

Refinement of the layer curves. The localized splines of degree 6 are similarly refined. With $\mathbf{p}^0_i$, $i = 0, 1, 2$ defined by $\mathbf{c}$ and $\mathbf{p}^1_i$, $i = 0, \ldots, 6$ the BB-coefficients of the next curve piece, we set $\mathbf{p}^0_i$, $i = 0, 1, 2$ in $\hat{\mathrm{p}}^0 := \sum_{i=0}^{6}(-1)^i\binom{6}{i}\mathbf{p}^0_{i1}$ according to (17) and $\ell^0 := \frac{1}{29}(36\mathbf{p}^0_2 + 6\mathtt{m}^0 - \mathtt{r}^0)$. Proceeding as when deriving (18) yields the local form

$$\mathbf{p}^0_{01} - 6\mathbf{p}^0_{11} + \frac{123}{29}\mathbf{p}^0_{21} + \frac{64}{29}\mathtt{m}^0 - \frac{64}{29}\mathtt{r}^0 - \ell^1 + \hat{\mathrm{s}}^0_{loc} = 0 \tag{26}$$

to calculate $\mathtt{m}^0$. The interaction with the input data is analogous to the sector-separating curves: apart from the ends we consider four consecutive pieces $\mathbf{p}^0, \mathbf{p}^1, \mathbf{p}^2, \mathbf{p}^3$ for the C^2 junction between $\mathbf{p}^1$ and $\mathbf{p}^2$. Proceeding as when deriving (18) but now leveraging also (20) yields a system of two linear equations of which we only display the relevant terms in $\ell^k, \mathtt{m}^k, \mathtt{r}^k \in \mathbb{R}$, $k = 0, 1, 2, 3$:

$$\begin{aligned}
&-\mathtt{r}^0 + (\frac{65}{48} - \frac{65}{36}\nu_1)\ell^1 + (\frac{11}{8} + \frac{5}{6}\nu_1)\mathtt{m}^1 + (\frac{145}{48} - \frac{145}{36}\nu_1)\mathtt{r}^1\\
&+ (\frac{145}{36}\nu_1 - \frac{193}{48})\ell^2 + (\frac{5}{8} - \frac{5}{6}\nu_1)\mathtt{m}^2 + (\frac{65}{36}\nu_1 - \frac{65}{48})\mathtt{r}^2\\
&+ \ldots = 0\,,\\
&(\frac{65}{48} - \frac{65}{36}\nu_1)\ell^1 + (-\frac{5}{8} + \frac{5}{6}\nu_1)\mathtt{m}^1 + (\frac{97}{48} - \frac{145}{36}\nu_1)\mathtt{r}^1\\
&+ (\frac{145}{36}\nu_1 - \frac{145}{48})\ell^2 + (\frac{21}{8} - \frac{5}{6}\nu_1)\mathtt{m}^2 + (\frac{65}{36}\nu_1 - \frac{65}{48})\mathtt{r}^2\\
&- \ell^3 + \ldots = 0.
\end{aligned}$$

These two equations are solved for $\mathtt{m}_1$ and $\mathtt{m}_2$ to complete the refinement formulas in terms of the free parameters ℓ and $\mathtt{r}$.

Appendix C. Proof of Proposition 1

The lemmas leading up to the proof repeatedly use the following simple argument, abbreviated (R): If f is a polynomial and g is a rational, then $h = f + g$ is rational.

Lemma 8 (along $\mathbb{c}^s, \mathbb{m}^s$). *If the BB-coefficients $\mathbf{t}_{ij}$ of the tensor-border $\mathbf{t}$ can be independently chosen and if both $\mathbf{t}$ and $\tilde{\mathbf{t}} := \mathbf{t}\circ\rho$ are polynomial, then the scalar functions a, b, d, e defining ρ in* (1) *are polynomials.*

Proof For $\mathsf{deg}(\mathbf{t}) = m$, the G^1 constraints (2) can be written as

$$\partial_v \tilde{\mathbf{t}}(u,0) = \underbrace{\sum_i^m a(u) B_i^m(u) m \mathbf{t}_{i1}}_{E_1(u)} - \underbrace{\sum_i^m a(u) B_i^m(u) m \mathbf{t}_{i0}}_{E_2(u)}$$
$$+ \underbrace{\sum_i^m b(u)(B_i^m(u))' m \mathbf{t}_{i0}}_{E_3(u)}$$

If we set all $\mathbf{t}_{ij}$ to zero except one $\mathbf{t}_{i1}$ for fixed i then the G^1 constraints (2) simplify to $\partial_v \tilde{\mathbf{t}}(u,0) = a(u) B_i^m(u) m \mathbf{t}_{i1}$ implying that $a(u)B_i^m(u)$ is a polynomial. If $a(u) := \frac{\overline{a}(u)}{\underline{a}(u)}$ is rational then the denominator $\underline{a}(u)$ must be a factor of $B_i^m(u)$ for all i. Since the gcd of the Bernstein polynomials is 1, this implies that $a(u)$ is a polynomial.

Since now $\partial_v \tilde{\mathbf{t}}(u,0) - E_1(u) + E_2(u)$ is a polynomial, by (R) so is $E_3(u)$, and by setting all $\mathbf{t}_{ij}$ to zero except for one $\mathbf{t}_{i0}$ for fixed i, we see that $b(u)(B_i^m(u))'$ must be polynomial for each i. Since the gcd of the $(B_i^m(u))' = \binom{m}{i}(1-u)^{m-1-i}u^{i-1}(i-mu)$ is 1, $b(u)$ must be a polynomial. Then, (R) applied to the G^2 constraints yields that $d\ \partial_v \mathbf{t} + e\ \partial_u \mathbf{t}$ is a polynomial and we can apply the same reasoning as for $a(u)$ and $b(u)$ to see that $d(u)$ and $e(u)$ are polynomial. |||

Now consider the sector-separating curves.

Lemma 9 (along $\mathbb{m}^s, \Phi$). *If both* $\mathbf{p}$ *and* $\vec{\mathbf{p}} := \mathbf{p} \circ \rho$ *are polynomial, and* $a(u)$ *in* $\rho(u,v) := (u + b(u)v, a(u)v)$ *is polynomial then* $b(u)$*,too, is polynomial.*

Proof Applying (R) to the G^1 constraint $\partial_v \vec{\mathbf{p}} := a\ \partial_v \mathbf{p} + b\ \partial_u \mathbf{p}$ when $a(u)$ is polynomial implies that $b(u)\partial_u \mathbf{p}(u,0)$ is polynomial. Presenting $\mathbf{p}(u,0)$ in BB-form of least degree (sector-separating curves may be of lower degree than the patches that join) and setting the corresponding independent coefficient of $\partial_u \mathbf{p}(u,0)$ to zero except for one, we conclude as in Lemma 8 that the denominator of $b(u)$ must be 1. |||

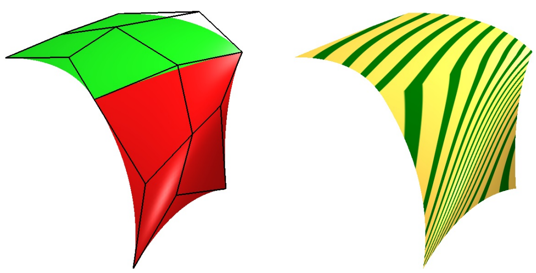

(a) BB-net (b) highlight lines

Figure 19: Example illustrating the need for the assumptions of Lemma 9: a polynomial G^1 two-patch bi-2 surface with rational $a(u)$ and $b(u)$.

The following example illustrates that it is necessary to demand that $a(u)$ be polynomial in order to prove Lemma 9. For $a(u) := \frac{-2}{2-u}$, $b(u) := \frac{2(1-u)}{2-u}$ and $\mathbf{p}$ and $\vec{\mathbf{p}}$ of degree bi-2, a solution of G^1-constraints (2) is

$$\vec{\mathbf{p}}_{01} := -\mathbf{p}_{01} + \mathbf{p}_{10} + \mathbf{p}_{00},\ \vec{\mathbf{p}}_{i0} := \mathbf{p}_{i0},\ i = 0,1,2;$$
$$\vec{\mathbf{p}}_{11} := -\mathbf{p}_{11} - \frac{1}{4}\mathbf{p}_{01} + \frac{7}{4}\mathbf{p}_{10} + \frac{1}{2}\mathbf{p}_{20},\ \vec{\mathbf{p}}_{21} := 3\mathbf{p}_{20} - 2\mathbf{p}_{21};$$
$$\mathbf{p}_{11} := \frac{1}{4}\mathbf{p}_{01} + \mathbf{p}_{21} + \frac{1}{4}\mathbf{p}_{10} - \frac{1}{2}\mathbf{p}_{20}.$$

Fig. 19 displays a concrete polynomial two-patch surface satisfying these G^1-constraints with rational functions $a(u)$ and $b(u)$.

Proof of Proposition 1. B-to-BB conversion transforms the 4×3 independently choosable control points of the surrounding bi-3 B-spline to 4×3 independently choosable BB-coefficients of the tensor-border $\mathbf{t}$, see Fig. 3 b. Therefore Lemma 8 proves (i); and since no bias implies $a(u) \equiv -1$, Lemma 9 proves (ii).